Atmos. Sci. Lett. (2017)
Published online in Wiley Online Library
(wileyonlinelibrary.com) **DOI:** 10.1002/asl.794

RMetS
Royal Meteorological Society

Intraseasonal variation of the East Asian summer monsoon associated with the MJO

Xinyu Li,[1,2,3] Gereon Gollan,[3,*] Richard J. Greatbatch[3,4] and Riyu Lu[1,2]

[1] *State Key Laboratory of Numerical Modeling for Atmospheric Sciences and Geophysical Fluid Dynamics, Institute of Atmospheric Physics, Chinese Academy of Sciences, Beijing, China*
[2] *University of the Chinese Academy of Sciences, Beijing, China*
[3] *RD Ocean Circulation and Climate Dynamics, GEOMAR Helmholtz Centre for Ocean Research Kiel, Kiel, Germany*
[4] *Faculty of Mathematics and Natural Sciences, University of Kiel, Kiel, Germany*

*Correspondence to:

G. Gollan, GEOMAR Helmholtz Centre for Ocean Research Kiel, Düsternbrooker Weg 20, 24105 Kiel, Germany.
E-mail: ggollan@geomar.de

Received: 8 August 2017
Revised: 17 October 2017
Accepted: 20 October 2017

Abstract

We investigate the daily variability of the East Asian summer monsoon (EASM) by projecting daily wind anomaly data onto the two major modes of an interannual multivariate Empirical Orthogonal Functions analysis. Mode 1, closely resembling the Pacific–Japan (PJ) pattern and referred to as PJ-mode, transits from positive to negative phase around mid-summer consistent with the Meiyu rains predominantly being an early summer phenomenon. Mode 2, which is influenced by the Indian summer monsoon (ISM) and referred to as ISM-mode, peaks in late July and early August and is associated with rainfall farther north over China. We then analyze the relation between the intraseasonal variation of the EASM and the Madden–Julian Oscillation (MJO) by analyzing circulation anomalies following MJO events. In the lower troposphere, the circulation anomalies associated with the MJO most strongly project on the PJ-mode. MJO phases 1–4 (5–8) favor the positive (negative) phase of the PJ-mode by favoring the anticyclonic (cyclonic) anomalies over the subtropical western North Pacific. In the upper troposphere, the circulation anomalies associated with the MJO project mainly on the ISM-mode.

Keywords: **intraseasonal variation; East Asian summer monsoon; MJO**

1. Introduction

The East Asian summer monsoon (EASM) is a distinctive component of the global climate system and brings summer rainfall to the most densely populated areas of the world. Variability of the EASM on different timescales is closely associated with summer floods and droughts over East Asia. Thus, understanding the variations of the EASM is of great socio-economic importance.

Several previous studies have described the interannual and decadal variability of the EASM in terms of multivariate Empirical Orthogonal Functions (MV-EOF) analysis (e.g. Wang *et al.,* 2008 ; Sun *et al.,* 2010 ; Wu and Zhou, 2016). The first EOF is closely related to the Pacific–Japan (PJ) pattern (Nitta, 1987) and is associated with rainfall anomalies along the East Asian rain band, including the Yangzte River valley. The second EOF is influenced by the Indian summer monsoon (ISM) (Greatbatch *et al.,* 2013) and is associated with a circumglobal teleconnection pattern (Ding and Wang, 2005) and rainfall anomalies over northern China. In what follows, we refer to EOF1 as the PJ-mode and EOF2 as the ISM-mode.

The EASM is also characterized by pronounced intraseasonal variability, in addition to the distinct interannual and interdecadal variability. The seasonal march of the EASM and the associated rain belts have been described by previous studies (e.g. Kang *et al.,* 1999; Chen *et al.,* 2004; Ding, 2007), which suggest that the PJ-mode and the ISM-mode also have distinct seasonal cycles. In the present study, we explore the daily variation of the EASM in terms of the circulation patterns associated with the major modes of interannual variability.

As the major mode of tropical intraseasonal variability, the Madden–Julian Oscillation (MJO; Madden and Julian, 1971), which propagates northeastward during summer with a dominant period of 30–90 days, plays a crucial role in the monsoon systems of East Asia (Yasunari, 1979; Zhang *et al.,* 2009; Chen *et al.,* 2015). These previous studies have documented that the MJO exerts an influence on rainfall over the EASM region, e.g. by influencing the western Pacific subtropical high and the associated moisture transport and vertical motions. In the second part of this study, we show a connection between the MJO and the intraseasonal variations of the EASM in terms of the patterns of the two major modes of interannual variability of the EASM. Note that the term 'MJO' is used here to describe the tropical intraseasonal oscillation during summer, though some authors also call it the 'boreal summer intraseasonal oscillation (BSISO)' (e.g. Kikuchi *et al.,* 2012; Chen *et al.,* 2015) and 'MJO' during winter.

The paper is arranged as follows: Section 2 describes the data and methods we use, Section 3 presents the results, and in Section 4, we provide a summary.

2. Data and methods

To obtain the two major modes of the interannual variability of the EASM, MV-EOF analysis is carried out over the EASM region (10°–50°N, 100°–150°E) following Sun *et al.* (2010). The data used here are June to August (JJA) seasonal mean zonal and meridional wind anomalies from the European Centre for Medium-Range Weather Forecasts Interim Reanalysis (ERA-Interim, Dee *et al.,* 2011) at 850 hPa and 200 hPa for the period 1979–2015. The detailed description of this method can be found in Text S1 in the Supporting information and in Sun *et al.* (2010). Daily variations of the two major modes are obtained by projecting daily wind data onto the corresponding spatial patterns of the two major EOF modes, respectively. The details of the projection process can be found in Text S2.

Precipitation data from the Climate Prediction Center Merged Analysis of Precipitation data (CMAP; Xie and Arkin, 1997) are also used. The real-time multivariate MJO index (RMM, available at http://www.bom.gov.au/climate/mjo/graphics/rmm.74toRealtime.txt) as defined by Wheeler and Hendon (2004) is used to quantify the MJO (See Text S3 for details). The MJO is divided into eight phases according to the angle spanned by its two components, RMM1 and RMM2, and the MJO amplitude is defined as $|\mathrm{MJO}| = |\mathrm{RMM1}, \mathrm{RMM2}| = [(\mathrm{RMM1})^2 + (\mathrm{RMM2})^2]^{1/2}$. We also test the robustness of our results by using other indices for the MJO (as in Kikuchi *et al.,* 2012; Kiladis *et al.,* 2014), and obtain similar results, especially for the relationship between the PJ-mode and the MJO, suggesting that our results are not sensitive to the choice of the index. (Results based on the Boreal Summer Intraseasonal Oscillation (BSISO, Kikuchi *et al.*, 2012) index, and slight differences in the results compared to the MJO index, are presented in the Supporting Information, Text S3, S4 and Figures S6–S8.)

The eight phases of the MJO are categorized as active phases when |MJO| is greater than or equal to 1.5, and the MJO is categorized as suppressed when |MJO|<=0.30 (this threshold yields similar sample sizes compared to the other categories), irrespective of the MJO phase.

3. Results

Figure 1 shows the first two MV-EOFs associated with the EASM that, respectively, explain 20.1 and 14.9% of the interannual variance and are well separated from higher modes according to North *et al.* (1982). The regression of CMAP JJA seasonal mean precipitation anomalies onto the corresponding normalized principal component time series of the two modes are also shown. As expected, the first mode resembles the PJ pattern (Nitta, 1987) at both 850 and 200 hPa. The positive phase of the PJ-mode is characterized by an anticyclonic anomaly over the subtropical western North Pacific (WNP) and a cyclonic anomaly over middle latitude East Asia at 850 hPa (Figure 1(a)). The WNP anticyclonic anomaly corresponds to a southwestward extension of the subtropical high and enhanced precipitation over the East Asian (Meiyu in China) rain band (Figure 1(a)). At 200 hPa, there is an anomalous cyclone centered around 135°E (Figure 1(b)). Associated with this cyclonic anomaly are anomalous westerly winds south of 40°N and anomalous easterly winds north of this latitude, corresponding to an equatorward displacement of the East Asian jet (Lin and Lu, 2005). The positive phase of the second mode (the ISM-mode) displays anomalous southerly winds extending northward and covering all of East China at 850 hPa and an anticyclonic anomaly centered around 120°E at 200 hPa (Figures 1(c) and (d)). This mode is influenced by the ISM (Greatbatch *et al.,* 2013). All of these results are very similar to those obtained by Sun *et al.* (2010).

We now project the daily wind anomalies, referring to the JJA seasonal mean, at 850 and 200 hPa onto the patterns of the two MV-EOF modes (see details in Text S2). The climatological seasonal cycles of the two modes are shown in Figure 2. The PJ-mode is characterized by a well-defined seasonal cycle. It transits from positive phase to negative phase, changing its sign in mid-summer. This climatological transition of the PJ-mode corresponds to the northward progression of the subtropical high in the lower troposphere and the East Asian jet in the upper troposphere and is associated with the occurrence of the Meiyu rains predominantly in early summer. The ISM-mode also seems to show a seasonal cycle, though not as strong as the PJ-mode. It transits from negative phase to positive phase around the beginning of July, and tends to transit to negative phase again near the end of August. This mode is associated with the tendency for rainfall in northern China to peak later than in the Meiyu rain band further south.

We now connect the intraseasonal variability of the two modes with the MJO. Figures 3(a) and (b) show the projection anomalies, referring to the daily mean climatological seasonal cycle (Figure 2), for the two EASM modes averaged over the first 5 days after each MJO phase occurs. The PJ-mode is closely related to the MJO (Figure 3(a)): Early MJO phases (1–4) are followed by the positive phase of the PJ-mode, the PJ-mode showing anomalies of roughly +1 standard deviation. Late MJO phases (5–8) are followed by the negative phase of the PJ-mode, the PJ-mode showing anomalies of up to −2 standard deviations, especially after MJO phases 6 and 7. The ISM-mode is associated with the MJO as well (Figure 3(b)): The positive phase of the ISM-mode follows MJO phases 3 and 4 and the suppressed MJO, while the negative phase of the ISM-mode follows MJO phases 7 and 8, with anomalies of up to −2 standard deviations.

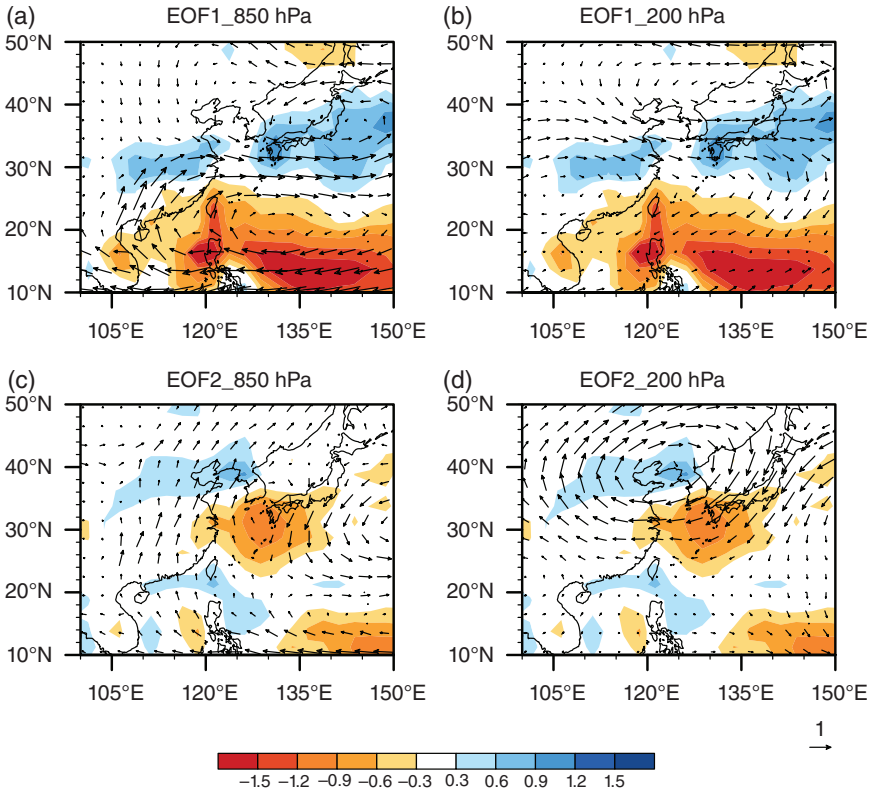

Figure 1. Spatial patterns of EASM interannual variability. (a and b) The first and (c and d) the second modes of an MV-EOF analysis on JJA seasonal mean (a and c) 850-hPa winds and (b and d) 200-hPa wind anomalies. Shading indicates the regression of CMAP seasonal mean precipitation anomalies (mm day^{-1}) onto the normalized time series of the two modes. The first mode is referred to as the PJ-mode and the second mode as the ISM-mode. The reference arrow in the lower right indicates a velocity anomaly of 1.0 m s^{-1}.

To analyze the relative importance of the wind anomalies at 850 and 200 hPa separately, we respectively project the daily wind anomalies at 850 and 200 hPa onto the corresponding spatial patterns of the two EASM modes. The projection anomalies averaged over the first 5 days after each MJO category occurs are shown in Figures 3(c)–(f). The MJO-related projection anomalies at 850 hPa for the PJ-mode (Figure 3(c)) are quite similar to those for both levels (Figure 3(a)). The anomalies at 200 hPa are weak and only significant after MJO phases 3 and 6 (Figure 3(e)), suggesting that the MJO-related circulation anomalies at 850 hPa are crucial for the strong projection onto the PJ-mode as seen in Figure 3(a).

The circulation anomalies at 850 hPa following MJO events project similarly on the ISM-mode, albeit weaker, as on the PJ-mode (Figures 3(c) and (d)), perhaps related to the fact that both the PJ-mode and the ISM-mode share anticyclonic anomalies over the subtropical WNP (Figures 1(a) and (c)). Furthermore, the circulation at 200-hPa is important for the MJO-related projection anomalies of the ISM-mode: MJO phase 4 is followed by the positive phase of the ISM-mode while MJO phases 7 and 8 are followed by a significantly enhanced occurrence of the negative phase of the ISM-mode (Figure 3(f)). The suppressed MJO also tends to favor the positive phase of the ISM-mode, projecting onto the ISM-mode mainly at 200 hPa in

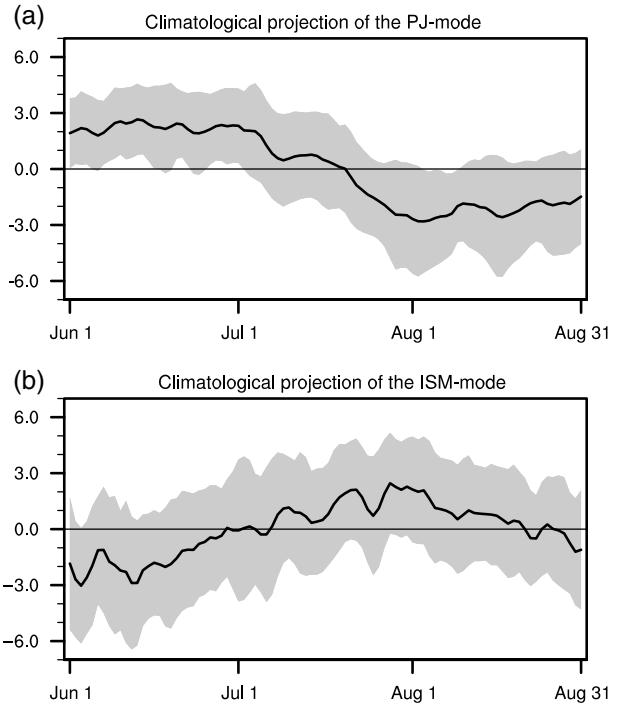

Figure 2. Daily climatologies of the projection of circulation anomalies, referring to the JJA seasonal mean (see Text S2 for additional details), onto the spatial patterns of (a) the PJ-mode and (b) the ISM-mode as shown in Figure 1. The gray shadings mark ±1.0 standard deviation of the projection values from 37 years (1979–2015).

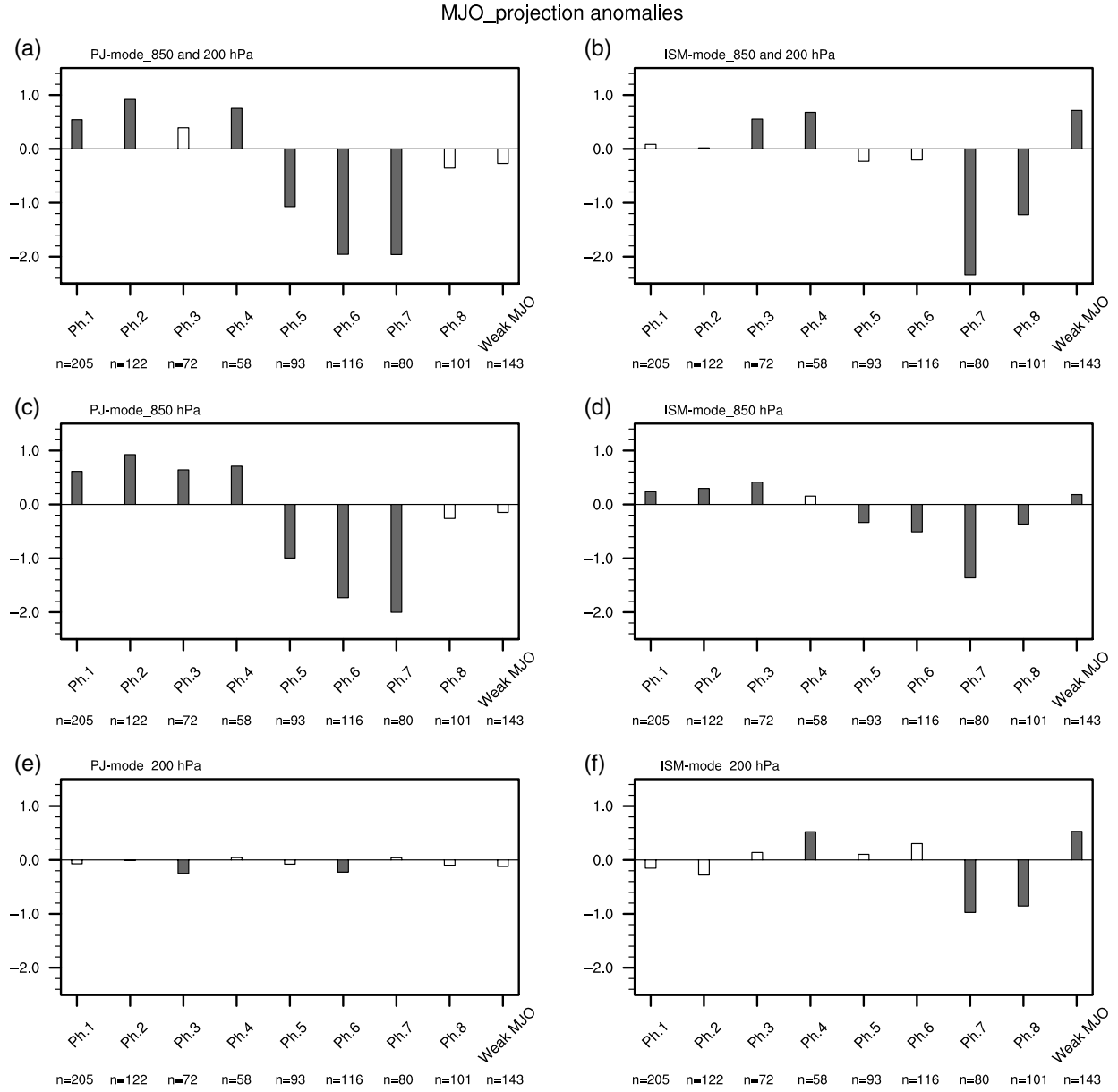

Figure 3. Daily projection anomalies for the two EASM modes, referring to the seasonal cycles shown in Figure 2, averaged over the 5 days following the occurrence of each of the 8 active MJO phases (Ph. 1 to Ph. 8) and the suppression of the MJO (weak MJO). (a and b) 850 and 200 hPa combined, (c and d) only 850 hPa, and (e and f) only 200 hPa. Shaded bars indicate composite anomalies that are significantly different from zero at the 0.05 level according to a two-tailed Student's *t*-test. '*n*' gives the number of days for each category.

the northern part of the domain (see Figure S1(i)). Although, for example, a suppressed MJO during winter is associated with anomalies like easterly wind above the equator (Gollan and Greatbatch, 2015), we cannot explain the anomalies seen here for a suppressed MJO. Overall, the atmospheric circulation in the EASM region after certain MJO phases mainly project on the PJ-mode at lower levels (Figures 3(c) and (d)) and the ISM-mode at upper levels (Figures 3(e) and (f)).

Figure 4 shows the 850-hPa wind and precipitation anomalies in the region of the Indian Ocean and western Pacific averaged over the first 5 days after the occurrence of each MJO phase. The corresponding figure for the 200 hPa is shown in Figure S1. Note that anomalies in Figure 4, as well as in Figure S1, refer to the JJA climatological seasonal mean. The anomalies in Figure 4 are consistent with those shown by previous studies (e.g. Wheeler and Hendon, 2004; Zhang *et al.,* 2009; Chen *et al.,* 2015). The evolution of the PJ-mode as the MJO evolves can be clearly seen: The anomalies in the EASM region show a clear positive phase of the PJ-mode after the occurrence of the early MJO phases (1–4). A significant anticyclonic anomaly appears over the subtropical WNP (Figures 4(a)–(d)) which is part of a large-scale anomalous lower-tropospheric easterly over the tropics flowing towards the enhanced precipitation over the Indian Ocean. The wind anomalies at 200 hPa associated with early MJO phases (Figures S1(a)–(d)) indicate a quasi-opposite flow over the tropics compared to 850 hPa, showing the zonal overturning

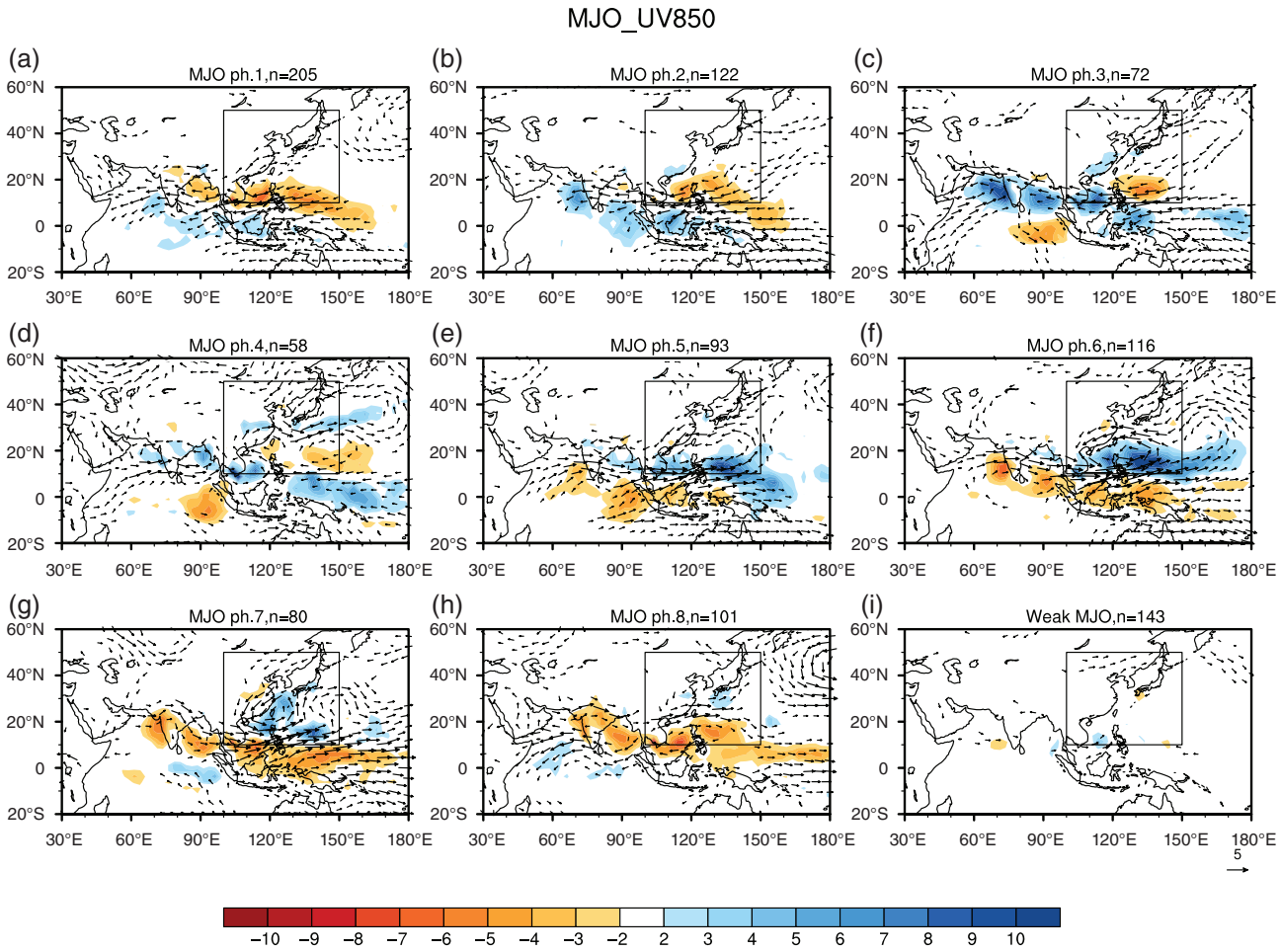

Figure 4. Anomalies of wind at 850 hPa (Vectors; Units: m s^{-1}) and precipitation (Shading; Units: mm day^{-1}) averaged over the 5 days following the occurrence of each of the eight active MJO phases and the suppression of the MJO. Anomalies here refer to the JJA seasonal mean. Only the composite anomalies that are significantly different from zero at the 0.05 level according to a two-tailed Student's *t*-test are shown. Vectors less than 1.0 m s^{-1} are omitted. The marked area represents the EASM region.

associated with the MJO. The downwelling branch of this overturning favors the suppressed precipitation over the tropical WNP, which can in turn favor the anticyclonic anomaly over the subtropical WNP (Nitta, 1987). Moreover, there are positive precipitation anomalies over southern China after MJO phases 2–4, that Zhang *et al.* (2009) relate to remote forcing via Rossby waves through a region of mean westerly winds (associated with the ISM). The wind and precipitation anomalies associated with late MJO phases (5–8) are almost opposite compared to early MJO phases, but the signal of reduced precipitation over southern China as found by Zhang *et al.* (2009) is weak here.

At 200 hPa (Figure S1), there is a significant cyclonic anomaly over northeast Asia after the occurrence of MJO phases 7 and 8, corresponding to the negative phase of the ISM-mode. The anomalies to the west of the EASM region resemble part of the circumglobal teleconnection pattern along the Asian westerly jet (around 40°N), which is associated with the suppressed precipitation anomalies over India (e.g. Ding and Wang, 2007; Moon *et al.,* 2013).

4. Discussion and conclusions

In this study, we explored the intraseasonal variability of the two major modes of the interannual variability of the EASM based on a MV-EOF analysis and investigated its relationship with the MJO. The first EOF is related to the PJ pattern (hereafter PJ-mode; Nitta, 1987) and the second EOF is influenced by the ISM (hereafter ISM-mode; Greatbatch *et al.,* 2013). The seasonal cycle of the PJ-mode favors the positive phase before mid-summer and then transits to negative phase, corresponding to the tendency for the Meiyu rains along the Yangtze River valley to occur predominantly in early summer. The ISM-mode seasonal cycle transits to the positive phase in July and August, associated with the occurrence of peak rainfall in northern China later in the season.

The PJ-mode at 850 hPa is closely associated with the evolution of the MJO. This connection mainly occurs at lower-tropospheric levels. Early/late MJO phases (1–4/5–8) are followed by the positive/negative phase of the PJ-mode by favoring an anomalous anticyclonic/cyclonic anomaly over the subtropical WNP. This anticyclonic/cyclonic anomaly is associated with

the suppressed/enhanced precipitation over the tropical WNP, which is favored by the MJO-related zonal overturning. The mechanism for the circulation anomalies over the subtropical WNP associated with the early MJO phases is also probably related to the eastward energy propagation by Rossby waves forced by the MJO-related heating center over the Indian Ocean through the low-level westerly waveguide (associated with the ISM), as suggested by Zhang *et al.* (2009). At upper levels, the MJO-related circulation anomalies mainly project on the ISM-mode, which is associated with a zonally oriented teleconnection pattern influenced by the precipitation anomalies over India for MJO phases 7 and 8.

Concerning the dynamical link between the EASM and the MJO, both ways of interaction are possible based on our results. However, by compositing circulation anomalies *after* MJO events, our results more likely suggest that the MJO influences the EASM. Furthermore, Sun *et al.* (2010) showed, using a linear baroclinic model, that diabatic heating in the tropical Indian Ocean region can drive the circulation patterns of the PJ-mode and the ISM-mode associated with the interannual variability of the EASM. Our findings concerning the relation between the MJO (at least for the active MJO) and the daily variation of the EASM are consistent with Sun *et al.* (2010) and suggest that a similar dynamical link as described by Sun *et al.* (2010) is present on intraseasonal timescales. The daily data used for our analyses (Figures 2–4) may contain variability that is not 'intraseasonal', e.g. synoptics or interannual variability. However, corresponding analyses based on 25–90 day band-passed filtered data agree well with the results presented here (see Figures S2–S5).

Taken together, these results show that there is significant information to be obtained about the EASM from knowing the phase of the MJO. Being able to predict the MJO therefore implies predictive skill for the EASM and, in particular, for intraseasonal rainfall anomalies over East Asia. Our results also suggest that any interannual variability of the MJO (e.g. Teng and Wang, 2003) could also influence the interannual variability of the EASM. These topics remain for future investigation.

Acknowledgements

XL is grateful to the Joint PhD Training Program (UCAS[2015]37) between the University of the Chinese Academy of Sciences and the Deutscher Akademischer Austausch Dienst (the German Academic Exchange Service) for supporting a 12-month stay at GEOMAR. Support is acknowledged from the German Federal Ministry of Education and Research (BMBF) through MiKlip2, subproject 01LP1517D (ATMOSMODINI). RJG is grateful for continuing support from GEOMAR. We gratefully thank two anonymous reviewers for helpful comments that improved the quality of the manuscript.

Supporting information

The following supporting information is available:

Figure S1. As Fig. 4, but showing 200 hPa winds.

Figure S2. As Fig. 2, but based on 25–90-day filtered data.

Figure S3. As Fig. 3, but based on 25–90-day filtered data.

Figure S4. As Fig. 4, but based on 25-90-day filtered data.

Figure S5. As Fig. S1, but based on the 25–90-day filtered data.

Figure S6. As Fig. 3, but using the BSISO index.

Figure S7. As Fig. 4, but using the BSISO index.

Figure S8. As Fig. S1, but using the BSISO index.

References

Chen T-C, Wang S-Y, Huang W-R, Yen M-C. 2004. Variation of the East Asian summer monsoon rainfall. *Journal of Climate* **17**: 744–762.

Chen J, Wen Z, Wu R, Chen Z, Zhao P. 2015. Influences of northward propagating 25–90-day and quasi-biweekly oscillations on eastern China summer rainfall. *Climate Dynamics* **45**: 105–124.

Dee DP, Uppala SM, Simmons AJ, Berrisford P, Poli P, Kobayashi S, Andrae U, Balmaseda MA, Balsamo G, Bauer P, Bechtold P, Beljaars ACM, van de Berg L, Bidlot J, Bormann N, Delsol C, Dragani R, Fuentes M, Geer AJ, Haimberger L, Healy SB, Hersbach H, Hólm EV, Isaksen L, Kållberg P, Köhler M, Matricardi M, McNally AP, Monge-Sanz BM, Morcrette J-J, Park B-K, Peubey C, de Rosnay P, Tavolato C, Thépaut J-N, Vitart F. 2011. The ERA-interim reanalysis: configuration and performance of the data assimilation system. *Quarterly Journal of the Royal Meteorological Society* **137**: 553–597.

Ding Y. 2007. The variability of the Asian summer monsoon. *Journal of the Meteorological Society of Japan* **85**: 21–54.

Ding Q, Wang B. 2005. Circumglobal teleconnection in the Northern Hemisphere summer. *Journal of Climate* **18**: 3483–3505.

Ding Q, Wang B. 2007. Intraseasonal teleconnection between the summer Eurasian wave train and the Indian monsoon. *Journal of Climate* **20**: 3751–3767.

Gollan G, Greatbatch RJ. 2015. On the extratropical influence of variations of the upper-tropospheric equatorial zonal-mean zonal wind during boreal winter. *Journal of Climate* **28**: 168–185. https://doi.org/10.1175/JCLI-D-14-00185.1.

Greatbatch RJ, Sun X, Yang X. 2013. Impact of variability in the Indian summer monsoon on the East Asian summer monsoon. *Atmospheric Science Letters* **14**: 14–19.

Kang I-S, Ho C-H, Lim Y-K, Lau K-M. 1999. Principal modes of climatological seasonal and intraseasonal variations of the Asian summer monsoon. *Monthly Weather Review* **127**: 322–340.

Kikuchi K, Wang B, Kajikawa Y. 2012. Bimodal representation of the tropical intraseasonal oscillation. *Climate Dynamics* **38**: 1989–2000.

Kiladis GN, Dias J, Straub KH, Wheeler MC, Tulich SN, Kikuchi K, Weickmann KM, Ventrice MJ. 2014. A comparison of OLR and circulation-based indices for tracking the MJO. *Monthly Weather Review* **142**: 1697–1715.

Lin Z, Lu R. 2005. Interannual meridional displacement of the East Asian upper-tropospheric jet stream in summer. *Advances in Atmospheric Sciences* **22**: 199–211.

Madden RA, Julian PR. 1971. Detection of a 40–50 day oscillation in the zonal wind in the tropical Pacific. *Journal of the Atmospheric Sciences* **28**: 702–708.

Moon JY, Wang B, Ha KJ, Lee JY. 2013. Teleconnections associated with Northern hemisphere summer monsoon intraseasonal oscillation. *Climate Dynamics* **40**: 2761–2774.

Nitta T. 1987. Convective activities in the tropical western Pacific and their impact on the Northern Hemisphere summer circulation. *Journal of the Meteorological Society of Japan* **65**: 373–390.

North GR, Bell TL, Cahalan RF, Moeng FJ. 1982. Sampling errors in the estimation of empirical orthogonal functions. *Monthly Weather Review* **110**: 699–706.

Sun X, Greatbatch RJ, Park W, Latif M. 2010. Two major modes of variability of the East Asian summer monsoon. *Quarterly Journal of the Royal Meteorological Society* **136**: 829–841.

Teng HY, Wang B. 2003. Interannual variations of the boreal summer intraseasonal oscillation in the Asian–Pacific region. *Journal of Climate* **16**: 3572–3584.

Wang B, Wu Z, Li J, Liu J, Chang CP, Ding Y, Wu G. 2008. How to measure the strength of the East Asian summer monsoon. *Journal of Climate* **21**: 4449–4463.

Wheeler M, Hendon HH. 2004. An all-season real-time multivariate MJO index: development of an index for monitoring and prediction. *Monthly Weather Review* **132**: 1917–1932.

Wu B, Zhou T. 2016. Impacts of the Pacific–Japan and circumglobal teleconnection patterns on the interdecadal variability of the East Asian summer monsoon. *Journal of Climate* **29**: 3253–3271.

Xie P, Arkin PA. 1997. Global precipitation: a 17-year monthly analysis based on gauge observations, satellite estimates, and numerical model outputs. *Bulletin of the American Meteorological Society* **78**: 2539–2558.

Yasunari T. 1979. Cloudiness fluctuations associated with the Northern Hemisphere summer monsoon. *Journal of the Meteorological Society of Japan* **57**: 227–242.

Zhang L, Wang B, Zeng Q. 2009. Impact of the Madden-Julian Oscillation on summer rainfall in southeast China. *Journal of Climate* **22**: 201–216.